Materials Research. 2022; 25:e20210574
DOI: https://doi.org/10.1590/1980-5373-MR-2021-0574

Polyvinyl Alcohol Films Loaded with Silver Nanostructures with Different Sizes and Shapes with Tuneable Plasmonic and Electric Properties. A Spectroscopic Study

Lourdes Araceli Granja[a,e], Nayely Pineda-Aguilar[b], Juan Pablo Saucedo-Vázquez[a], Gottfried Suppan[a], Cristóbal Lárez-Velázquez[c], Salomé Galeas[f], Gema González[d], Floralba López[a]*

[a]*Universidad Yachay Tech, Escuela de Ciencias Químicas e Ingeniería, CATS-Catalysis Theory and Spectroscopy, 100119, Urcuquí, Ecuador.*
[b]*Centro de Investigación en Materiales Avanzados S.C. (CIMAV), Subsede Monterrey, Alianza Norte 202, Parque de Investigación e Innovación Tecnológica, C.P. 66628 Apodaca, Nuevo León, México.*
[c]*Facultad de Ciencias, Departamento de Química, Laboratorio de Polímeros, 5101, Mérida, Venezuela.*
[d]*Universidad Yachay Tech, Escuela de Ciencias Físicas y Nanotecnología, 100119, Urcuquí, Ecuador.*
[e]*Instituto Superior Tecnológico 17 de Julio, Urcuquí, Ecuador.*
[f]*Laboratorio de Nuevos Materiales (LANUM), Escuela Politécnica Nacional, Quito, Ecuador.*

Received: November 12, 2021; Revised: March 11, 2022; Accepted: May 05, 2022

To study the effect of the incorporation of silver nanoparticles into polyvinyl alcohol (PVA) films on their optical and conducting properties, silver nanostructures with different sizes covering from spherical to polyhedral shapes were synthesized and embedded into the polymer. The sizes of the obtained silver nanostructures were analyzed by Dynamic Light Scattering (DLS), which exhibited high stability, attributed to their surface potential. Multimodal distributions suggest changes in shape ranging from spheres (~40 nm) to prisms (~100 nm), which was confirmed by Scanning Electron Microscopy (STEM/SEM) analysis. By embedding these nanostructures in polyvinyl alcohol (PVA), AgNPs loaded PVA polymer films were prepared, exhibiting a hypsochromic shift in the surface plasmon resonance band of the nanostructures. For conductivity determination of AgNPs loaded PVA polymer films, Electrochemical Impedance Spectroscopy (EIS) was used. The results indicated that the conductivity of the samples is highly dependent on the size and shape of the AgNPs embedded into the polymer, resulting in higher conductivity for smaller silver nanostructures.

Keywords: *Silver nanostructures, Plasmon bands, Electrochemical Impedance, Nanocomposites.*

1. Introduction

Interest in nanoscience has been growing in recent years, especially due to the nanotechnological advantages displayed by systems on this scale, arising from their high surface/volume ratio that give them distinctive properties[1-3]. Among nanostructured systems, silver nanostructures (AgNPs) stand out for their optical, electrical, magnetic and catalytic properties that depend on their size and shape, and are very different from those of their bulk phases[4,5] allowing for potential applications, such as chemical and/or biological sensing, catalytic pollutant removal, antimicrobial applications, medical and therapeutic benefits[6,7].

The combination of nanomaterials with a polymer matrix for the preparation of composite materials, called hybrids or nanocomposites[8], allows modulating the properties of precursor materials to tailor them for specific applications. In particular, conductive polymer composites have a key role in the development of electronic devices such as flexible screens[9] and in the manufacture of electrochemical and flexible energy storage and conversion devices, among others[10,11] while maintaining synthetic feasability[12] and low production costs[13].

Polyvinyl alcohol (PVA) has become a material with high potential for interesting applications due to its low toxicity, low cost, solubility in water, optical transparency, high biocompatibility, and biodegradability (both under aerobic and anaerobic conditions)[14]. Incorporating metal nanoparticles in a polymer matrix inhibits their agglomeration, not only by hindering the diffusion of the particles, but the polymer matrix also acts as a stabilizing agent of the surface[15]. The combination of PVA with suitable materials can generate an increase in its conductivity and improves its dielectric behavior[16-19]. For example, the doping of PVA films with ZnO-NPs result in a significant increase in their AC and DC conductivities, making these materials potential candidates for electronic applications[20]. PVA films doped with AgNPs have also been previously reported, AgNPs were synthesized using the traditional reducing agent sodium borohydride. Conductivities of the doped films showed significant increases in ionic conductivity as NPs concentration in the films was increased[21].

The aim of this work is to evaluate the effect of the presence of AgNPs with different sizes and shapes on the conductivity of thin PVA films, as well as the encapsulation capacity of PVA. AgNPs were prepared

*e-mail: agranja@ist17dejulio.edu.ec

following a previously reported method[22], optimizing colloidal chemical synthesis conditions to promote the formation of nanostructures with different sizes and shapes. Some characterization techniques, such as UV-vis, DLS, STEM/SEM were carried out to determine the size and shape of the nanostructures, and the conductivity of the nanocomposite was measured by EIS. Although the nanocomposites containing AgNPs with polymers have been reported before, detailed studies considering the effect of shape (morphology) and size on the conductivity are scarce, albeit this being a fundamental property in different applications.

2. Experimental

2.1. Materials

Analytical grade reagents were purchased from Sigma Aldrich (silver nitrate, sodium borohydride, hydrazine, sodium citrate) and from LobaChem (polyvinyl alcohol) and used without further purification.

2.2. Synthesis and characterization of silver nanostructures

Synthesis and characterization of silver nanostructures were carried out following the procedure described by Power et al.[22]. Briefly, an initial seed solution was prepared mixing by magnetic stirring 10 mL of 2.5 mM sodium citrate (SCT) and 10 mL of 3 mM $AgNO_3$ until homogenization was achieved, and then 6 mL of 1 mM sodium borohydride ($NaBH_4$) were added dropwise. The resulting solution was labeled Solution A. Subsequently, 5 mL of an aqueous solution of PVA 5% wt.,1 mL of Solution A, 3 mL of 1 mM SCT, and 5 mL of 0.1 M hydrazine were added under constant stirring, forming Solution B. Finally, additional volumes of 1 mM $AgNO_3$ were slowly poured to Solution B, maintaining constant stirring, to obtain AgNPs samples to be evaluated. The synthesis of the AgNPs was carried out at room temperature (~23 °C), generating colloidal dispersions with a pH = 9. The silver concentration in each of the dispersion samples ranged between 0.010 and 0.015 mM, as indicated in Table 1.

2.3. Preparation of PVA films embedded with AgNPs

The films were prepared by mixing a 5% wt. PVA solution and the sols of previously prepared AgNPs in a 70:30 volume ratio with constant stirring until a visually homogeneous mixture was obtained. The resulting mixtures were poured into plastic Petri dishes of 5 cm in diameter, and placed in an oven at 40 °C for 24 hours for evaporation of the solvent. Once the films were dry, they were detached from the Petri dishes and stored at room temperature.

2.4. Characterization of silver nanostructures

2.4.1. UV-vis Spectroscopy

The respective surface plasmon absorption bands of the different dispersions were obtained by a Perkin Elmer model LAMBDA 1050 spectrometer, with a measurement range of 175 - 3300 nm). The samples were analyzed in a 1 cm optical path quartz cuvette.

2.4.2. Electron Microscopy

The morphological analysis of the AgNPs was performed by Scanning Electron Microscopy (SEM) using a Phenom World brand PhenomProX microscope. In addition, SEM studies were carried out with a transmission detector (STEM) by means of Nova Nano SEM200 equipment, in low vacuum mode, using an XT detector (STEM). For this analysis, three drops of the sample were dispersed in 2 mL of isopropanol with ultrasound treatment for 5 minutes; then a drop of the dispersion was taken and placed on a Lacey Carbon Type-A copper grid (300 mesh) to be allowed to dry at room temperature.

2.4.3. Dynamic Light Scattering

DLS is the standard technique to determine the hydrodynamic size distribution (in the range of nanometers and micrometers) and evaluate the stability of the nanostructures in the colloidal dispersions. The analysis was carried out using the Brookhaven, 90 Plus, Particle Size Analyzer equipment.

Table 1. Silver concentrations [Ag] of different colloidal dispersions prepared with different volumes of $AgNO_3$ (V_{AgNO3}) whose main ($\lambda_{max,1}$) and secondary ($\lambda_{max,2}$) maxima of their plasmon bands are indicated. Labels for each prepared sample are also indicated.

Label	V_{AgNO3} (mL)	[Ag] in sample (mM)	Dispersion Color	$\lambda_{max,1}$ (nm)	$\lambda_{max,2}$ (nm)
AgNP-00	0	0.01	Yellow	416	---
AgNP-10	1.0	0.013	Orange	430	---
AgNP-20	2.0	0.013	Red	437	---
AgNP-30	3.0	0.015	Purple	482	424
AgNP-35	3.5	0.015	Blue Purple	502	432
AgNP-40	4.0	0.015	Blue	515	426
AgNP-45	4.5	0.015	Light Blue	533	428
AgNP-50	5.0	0.015	Blue Green	551	425
AgNP-55	5.5	0.015	Turquoise 1	571	424
AgNP-60	6.0	0.015	Turquoise 2	612	436
AgNP-65	6.5	0.014	Green	632	444

2.4.4. Electrochemical Impedance Spectroscopy

For the determination of the electrical parameters of the pure and AgNPs loaded PVA films, Electrochemical Impedance Spectroscopy (EIS) was used. For this, a Metrohm potentiostat model Autolab PGSTAT302N was used. This is an interesting, non-destructive, and widely used electrochemical measurement technique in fields such as electrochemistry, materials science, biology, and medicine[23]. EIS is based on the use of an alternating potential signal to determine the system's current response. For the analysis, the film samples were sandwiched between conductive carbon electrodes to be evaluated. The geometric electrode area (denoted by *A*) and thickness (denoted by *d*) of each evaluated film were recorded using a vernier micrometer so all impedance spectra can be normalized to the unit area. For all EIS measurements, an excitation potential signal with an amplitude of 0.1 V around the open cell potential (OCP) was applied and the excitation frequency was varied between $1x10^{5}$ and $1x10^{-1}$ Hz.

3. Results and Discussion

3.1. Optical characterization of AgNPs sols

The colloidal feature of the obtained dispersions was evidenced by the Tyndall effect exhibited, an effect that is not seen in solutions. Depending on the amount of $AgNO_3$ involved in the dispersions, the AgNPs sols presented different colorations, which were obtained after continuously adding specific increments of volumes of 1 mM $AgNO_3$ to Solution B, initially light yellow-brown in color. The composition, color, and labeling of each dispersion are indicated in Table 1.

In Figure 1 (top) the obtained sols exhibiting different colors, changing from yellow (lowest amount of $AgNO_3$) to green (highest amount of $AgNO_3$), are shown. All the obtained dispersions exhibited long stability over time, as they maintained their coloration for several months. All obtained colloidal dispersions showed strong light absorption in the UV-vis region. The normalized UV-vis spectra obtained from these samples are depicted in Figure 1 (bottom). UV-vis spectra and the colors of these dispersions can be related to specific shapes of the AgNPs as has been previously reported[24,25].

The incident light in this type of nanomaterials induces a collective oscillation of the conduction electrons, whose resonant frequency depends on the size, shape, composition, orientation, and local dielectric environment of the nanostructures[24,26]. In the UV-vis spectra of the obtained AgNPs dispersions a clear bathochromic shift of the plasmonic band is observed, with a variation in the wavelength associated with the maximum of the main band that ranges from 416 to 640 nm. The initial absorbance data were normalized for a better comparison. In Table 1 the values of the wavelengths corresponding to the maxima of the plasmon absorption bands of each of the colloidal dispersions of AgNPs are specified. The shift in the wavelength of the maximum of these bands has usually been associated with variations in the size and shape of the particles[22]. For AgNP-30 to AgNP-65 samples spectra the appearance of two additional bands (~330 and ~400 nm) can

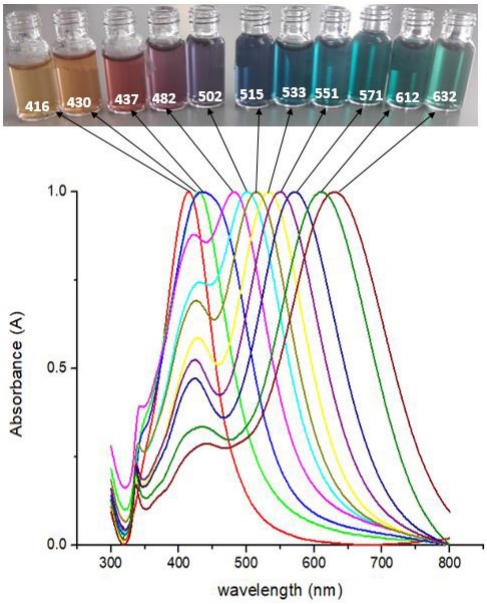

Figure 1. Shift plasmon absorption bands for colloidal dispersions of AgNPs. From left to right: AgNP-00 (416 nm), AgNP-10 (430 nm), AgNP-20 (437 nm), AgNP-30 (482 nm), AgNP-35 (502 nm), AgNP-40 (515 nm), AgNP-45 (533 nm), AgNP-50 (551 nm), AgNP-55 (571 nm), AgNP-60 (612 nm), AgNP-65 (632 nm).

be attributed to the presence of AgNPs of different sizes and shapes in the same colloidal dispersion[27,28].

The different colorations of the colloidal dispersions, and thus the wavelength of the plasmon absorption maximum, are reached by appropriate adjustments in the synthesis of AgNPs and are in good agreement with similar systems previously reported[29-31]. These wavelength values correspond to a specific geometry of the nanostructures. Changes in geometry from spherical nanoparticles to nanoprisms imply a variation in their aspect ratio ($R_{w/h}$), that is, in the width/height ratio of the structures. As $R_{w/h}$ increases, the maximum of the plasmonic bands experiences a bathochromic shift, related to the enhancement of the local electromagnetic field associated with AgNPs. Particularly for colloidal AgNPs of different sizes and shapes, Emory and Nie demonstrated large field enhancement factors associated with different forms of AgNPs[32,33].

3.2. Morphological analysis of the AgNPs.

The morphological features of the AgNPs were examined by STEM/SEM. Figure 2 shows a micrograph obtained by SEM for the AgNP-65 whose colloidal dispersion presented a blue-green coloration ($\lambda_{max,1}$ = 632 nm), characteristic of silver structures referenced as nano-polyhedra[34]. As can be seen from this figure, most of the AgNPs have different sizes (in the range of 50 - 150 nm), which is consistent with the bandwidth of plasmon absorption bands observed in UV-vis spectra.

Changes of the size and shape of AgNPs, shown in Figure 3, are achieved during chemical synthesis involving nucleation and growth of silver nanostructures. The initial nucleation mechanism involves $NaBH_4$ and SCT, which

were used as reducing and capping agents, respectively, although some previous reports confer to SCT a reducing capacity[35]. Subsequently, the growth process controlled by diffusion involves hydrazine as a reducing agent, and SCT as a capping agent.

Figure 3a) corresponds to the sample AgNP-20, a dispersion of red color with a $\lambda_{max,1}$ = 437 nm. The predominantly spherical morphology observed in the STEM/SEM micrograph shown in Figure 3a)-left, as well as the size distribution obtained by DLS and shown in Figure 3a)-right, suggests three populations of particles with average sizes of 2, 9 and 70 nm, respectively. It is assumed that the formation of spherical particles is due to the low concentration of Ag^+ in solution and to the initial stage of growth.

Figure 3b)-left shows a STEM/SEM micrograph for the sample AgNP-40, a dispersion of blue color with a $\lambda_{max,1}$ = 515 nm, is shown. Quasi-spherical shapes remain predominant; however other types of structures are observed as well, some of them being more elongated (or ellipsoidal) and others with truncations. The size distribution, shown in Figure 3b)-right, reveals the presence of particles with average diameters around 15 and 100 nm. Greater sizes than those observed in Figure 3a, for sample AgNP-20, could be a consequence of a secondary Ostwald ripening growth mechanism, whereby the smallest particles are added to the largest ones[36,37].

Finally, Figure 3c)-left shows the STEM/SEM micrograph for sample AgNP-65, a dispersion of green color with a $\lambda_{max,1}$ = 632 nm. In this figure, the presence of structures with interesting anisotropic geometries is observed, showing more elongated structures and prismatic shapes. These and other shapes, such as planar triangles, have been previously reported and associated with the higher stability acquired by the particles formed by this method, especially in an advanced growth stage[38]. In the growth process of silver nanostructures defects can be generated due to the anisotropic deposition (or incorporation) of silver atoms in the initial spherical seeds, which leads to values of $R_{w/h}$ different from one. Variations in $R_{w/h}$ imply loss of spherical symmetry of the structure due to growth on preferential sides or truncation on others, generating faceted particles in the case of larger nanostructures, for which the main plasmon absorption band shifts to red[26,31,39-41] as was shown by UV-vis (Figure 1). Although the way in which these crystal lattice defects affect the resulting shape of the AgNPs has not been studied in detail, this mechanistic proposal seems to justify their different characteristics, such as color, maximum in the plasmon absorption band, and morphology[31,41].

The $R_{w/h}$ ratio of the observed latter structures is obviously different from one, which could explain the appearance of average sizes around 1.5 and 7 nm in the size distribution, in addition to the main peak at ~100 nm. It is worth mentioning that particle size measurements by DLS are based on the scattering of an incident light beam, making use of the Stoke-Einstein (SE) equation along with other related approaches[42], the hydrodynamic radii of the nanostructures is determined. Although these approaches are very useful to evaluate the dynamic behavior of nanostructured systems, and from this their spatial dimensions, a spherical geometry of particles is assumed, and therefore the results obtained could be controversial. For example, for non-spherical particles, the peak associated with a smaller hydrodynamic diameter is attributed to the rotational diffusion of the nanostructures instead of an actual dimension of them, as is also suggested in previous studies[43].

From the obtained results from DLS and STEM/SEM, the size and shape of the prepared AgNPs are consistent with those obtained from UV-vis spectroscopy. In Table 2 the average size determined by DLS analysis for some of the prepared AgNPs is shown, also indicating the maximum of the main plasmonic band to note the aforementioned redshift trend as the nanostructures grow.

3.3. Studies with AgNPs loaded PVA films

Figure 4 depicts the obtained AgNPs loaded PVA films. Clearly, each film prepared from different AgNPs dispersions exhibited distinguishable colors. The colors of the films were different from those of their precursor AgNPs dispersions, exhibiting a slight hypsochromic shift, that is, a shift of the $\lambda_{max,1}$ towards lower wavelength values as can be seen for the samples depicted in Figure 4a) to Figure 4d). As the characteristic gray color of bulk silver is not observed for any of the prepared films, it is suggested that the polymer matrix prevented agglomeration of the AgNPs[44].

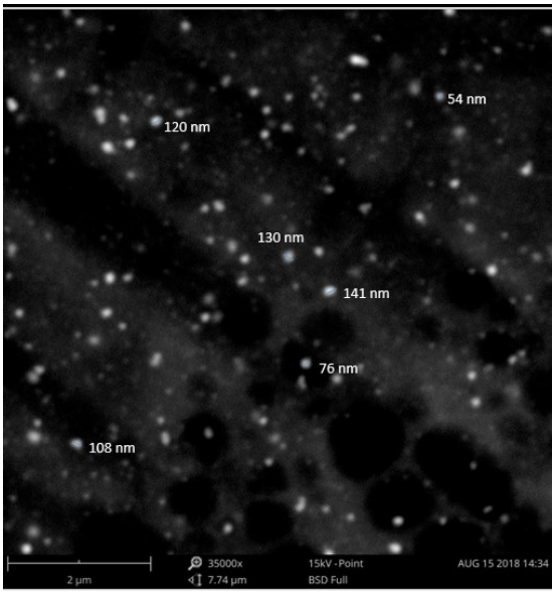

Figure 2. Micrograph obtained by SEM for AgNP-65 sample ($\lambda_{max,1}$ = 632 nm).

Table 2. Average sizes of some AgNPs obtained from DLS analysis along with the maximum of the main plasmon absorption band ($\lambda_{max,1}$) for each one of them.

CODE	$\lambda_{max,1}$ (nm)	Size of AgNPs (nm)	Polydispersity
AgNp-00	416	41.72	0.647
AgNp-20	437	44.80	0.356
AgNp-35	502	80.80	0.316
AgNp-40	515	82.40	0.476
AgNp-55	571	91.93	0.685
AgNp-65	632	104.3	0.227

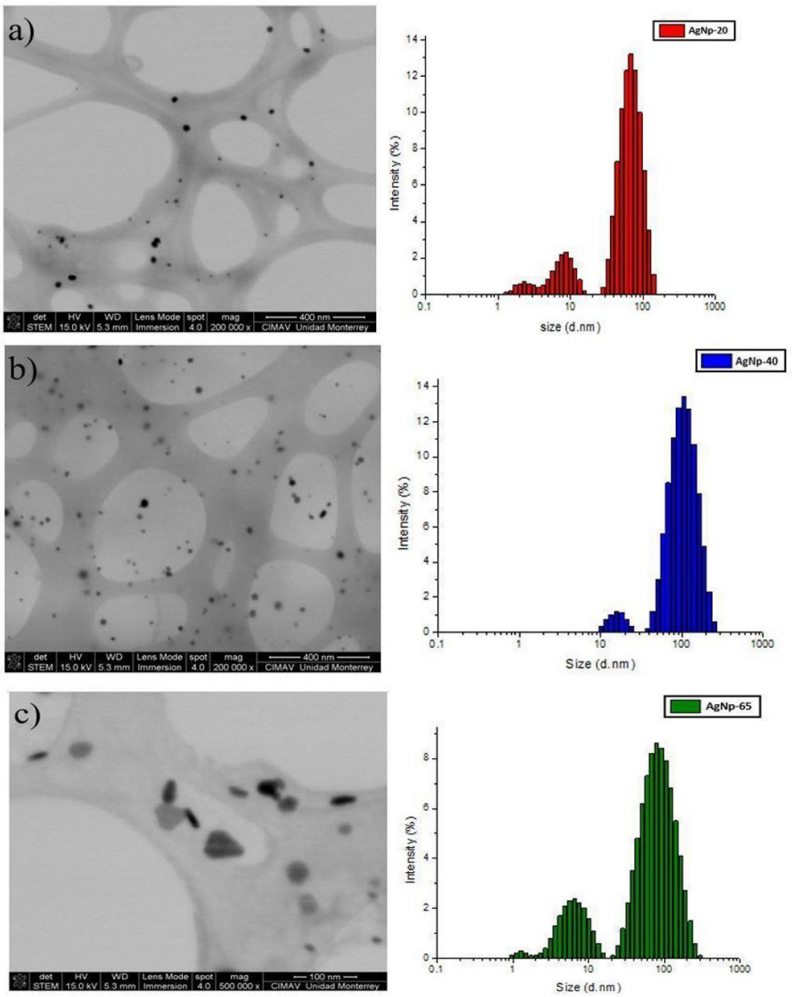

Figure 3. STEM/SEM micrographs (left) and particle size distribution (right) of AgNPs with the maxima of the plasmon absorption band at a) 437 nm, b) 515 nm and c) 632 nm.

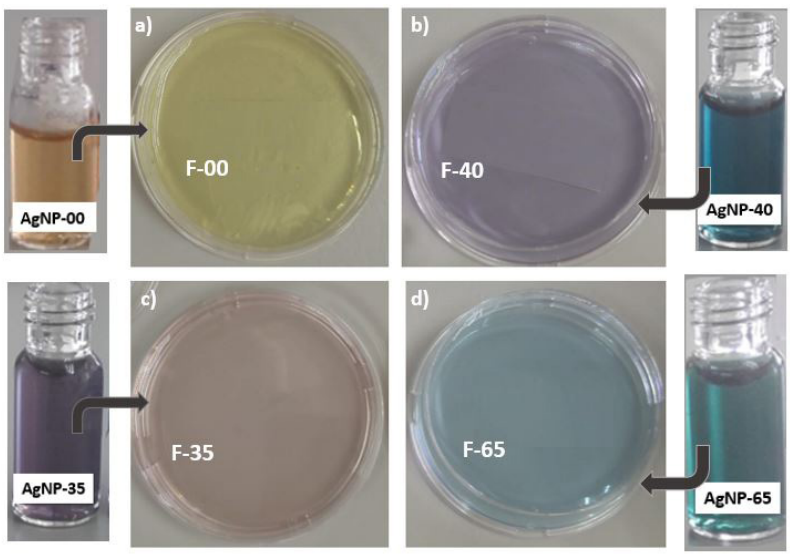

Figure 4. Different AgNPs loaded PVA films prepared from precursor AgNPs dispersions indicated next to each film.

3.4. Electrochemical impedance spectroscopy for AgNPs loaded PVA films

The electrical responses of PVA-based thin films were obtained from EIS analysis. Experimental impedance data were fitted to the equivalent electrical circuit models shown at the top of Figure 5.

The total impedance of pristine PVA films can be well described by a simple Randless circuit[45], as described in Figure 5, whereas the total impedance of metal AgNPs loaded polymer films can be fundamentally represented by three contributions[46,47]: (i) the film resistance (R_s) representing the impedance of the loaded thin film, (ii) the impedance of the charge-transfer between the electrode and thin film, where the charge transfer resistance is denoted by R_I, and finally (iii) a constant phase element, denoted by CPE_I, attributed to a frequency dispersion originated form a surface disorder or inhomogeneity of the electrode surface, accounted by the exponential factor N in the impedance equation of a constant phase element as given by Equation 1[48]:

$$Z_{CPE} = (1/Y_0)(j\bullet\omega)^{-N} \quad (1)$$

where Z is the impedance of the CPE element, Y_0 is a constant, j is the imaginary number, ω is the angular frequency, and N the exponential factor with $N< 1$ for a CPE.

The third contribution is associated with charge transfer between metallic nanostructures' grain boundaries and the polymer film, where R_{GB} represents the charge transfer resistance between the particles and the polymer film, and CPE_{GB} has the same phenomenological origin as CPE_I, but it is attributed to the NPs' surface[48].

Hence, the total impedance of the Randles circuit shown on the left of Figure 5a) can be given by[48]:

$$Z = R_S + 1 / [1/R_I + Y_I\bullet(j\bullet\omega)^{NI}] \quad (2)$$

where R_s is the film resistance, R_I the charge transfer resistance film-electrode, Y_I and N_I a constant and the exponential factor attributed to the ionic contribution of CPE_I according to Equation 1, respectively, and the other symbols retain their previously defined meaning.

Furthermore, the total impedance of the AgNP loaded PVA films can be expressed by Equation 3:

$$Z = R_S + 1 / [1/R_I + Y_I\bullet(j\bullet\omega)^{NI}] + 1 / [1/R_{GB} + Y_{GB}\bullet(j\bullet\omega)^{NGB}] \quad (3)$$

where R_{GB} is the charge transfer resistance film-NPs, Y_{GB} and N_{GB} a constant and the exponential factor attributed to the contribution of the grain boundaries of CPE_{GB}, respectively.

The Nyquist plots (-Z" vs. Z') are shown in Figure 5b) describing the frequency response of the PVA films for different loading with AgNPs of different sizes and shapes, as well as the corresponding fitting of the data to Equation 2 and Equation 3. It can be observed that the impedance of the AgNP loaded thin films decreases as the size of the AgNPs used for doping also decreases, thus the sample with the highest impedance is the one prepared from PVA and AgNP-60 samples with a $\lambda_{max,1}$ = 632 nm. The lowest value of impedance corresponds to the film with the smallest nanoparticles (AgNP-00), those that present a $\lambda_{max,1}$ = 416 nm. The results shown in Table 3 indicate that loading with AgNPs contributes significantly to decreasing the impedance of PVA films. The results also

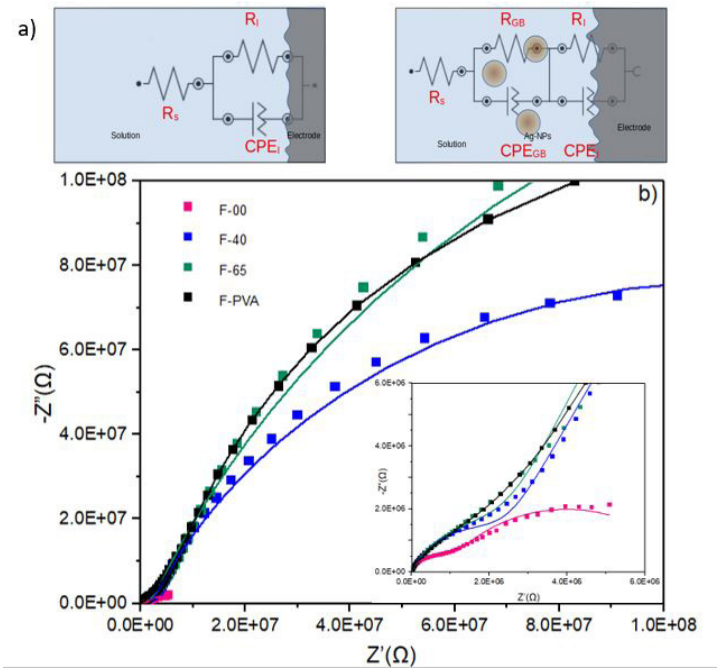

Figure 5. a): Schematic representation of the electrochemical cell and the proposed electric equivalent circuits for pristine PVA films (left), and AgNP loaded PVA films (right). b): Nyquist plot for pristine PVA films and films loaded with different AgNPs showing in the inset the magnification of the high-frequency region. Symbols: experimental data. Continuous lines: fits using the suggested equivalent cycles.

indicate that the larger the size of the NPs, the greater the R_1, obtaining values ranging from 6.05×10^6, 225.0×10^6, and 422.0×10^6 Ohm for those films formed from samples labeled as F-00, F-40, and F-65, respectively, as is indicated in Table 3. This increase in impedance is due to the lower number of free Ag^+ ions that stem from the-oxidative dissolution of metallic silver on the surface of the larger NPs. Oxidative dissolution is a highly exergonic process, which can lead to the release of Ag^+ in aerated systems, the oxidation of AgNP being thermodynamically favorable to oxidize at atmospheric oxygen pressures[49]. In comparison to their larger prism-shaped counterparts, smaller spherical NPs have a higher surface-to-volume ratio, which leads to greater susceptibility to oxidation. As a consequence, more Ag^+ can be formed from Ag^0, increasing the number of free ions and reducing R_1 as particle size decreases[46].

Whereas the contribution to the total impedance originating from the grain boundaries in terms of R_{GB} increases only slightly as the size of the AgNPs increases, Y_{GB} decreases. This is caused by a reduction in the absolute number of grains as smaller grains agglomerate to larger particles and therefore reducing the effective grain boundary-electrolyte interface area, which can also be considered by the change in N_1. In a simple plate capacitor model, the capacitance C is proportional to the electrode area (which in this case is represented by the grain boundary- electrolyte interface) by the following relationship:

$$C = e_r \bullet e_0 \bullet A / l \tag{4}$$

where ε_r is the relative permittivity, ε_0 the permittivity in vacuum, A the electrode area of the capacitor and l the distance between the capacitor plates.

The values of R_s were obtained from the impedance spectra, which in turn allows to calculate their specific conductivity (σ) through Equation 5:

$$\sigma = d / Rs \bullet A \tag{5}$$

where d is the thickness of the film and, as mentioned before, A is the area of the sample.

Surprisingly enough, the pristine PVA thin film shows a lower impedance than the sample prepared with the largest AgNPs. This can be explained by examination of the parameters obtained for PVA and sample F-65 shown in Table 3. The incorporation of large AgNPs also introduces the contribution by the grain boundaries along with a small Y_{GB}, which in turn introduces a large impedance component according to Equation 3. However, a calculation of the specific conductivity, which is a value normalized by cell and film geometry, the value obtained for the conductivity of the pristine PVA film is 1.71×10^{-9} S cm^{-1}, which is comparable with the value of 4.45×10^{-9} S cm^{-1} reported by Devikala[45]. However, the conductivity of PVA films varies in the literature depending on the molecular weight[50].

For example, Rithin et al.[51] reported a conductivity value for PVA films of 1.05×10^{-11} S cm^{-1}, which is in the same order of magnitude as 1.38×10^{-11} S cm^{-1}, the value reported by Mahendia et al.[52], but also values as low as 6.11×10^{-14} S cm^{-1} have been reported[53].

As can be observed in Table 4, PVA films loaded with AgNPs show conductivity values up to 20 times greater than the non-loaded PVA film, as is the case for the sample with $\lambda_{max,1}$ = 416 nm.

The data depicted in Table 4 show that the conductivity and the size of the charged AgNPs, that is, the smaller the NPs, the greater the conductivity. This is due to the silver ions (Ag^+) found on the surface of the smallest nanostructures, which increase the number of charge carriers in the polymeric matrix, consequently reducing the films impedances[46]. As the silver nanostructures grow, these ions are reduced to Ag^0, effectively removing mobile charge carriers from the film and raising the impedance of the film.

Table 3. Fitting parameters obtained from EIS analysis for the model given by Equation 2 and Equation 3 for different AgNP loaded PVA films evaluated.

SAMPLE	R_s (Ohm)	R_{GB} (Ohm)	Y_{GB} (Mho* s^N)	N_{GB}	R_I (Ohm)	Y_I (Mho* s^N)	N_I
PVA	$6.56x10^3$			0.839	$2.93x10^6$	$7.94x10^{-10}$	0.839
F-00	$1.81x10^3$	$0.97x10^6$	$12.1x10^{-9}$	0.855	$6.05x10^6$	$138x10^{-9}$	0.736
F-40	$5.36x10^3$	$2.14x10^6$	$5.94x10^{-10}$	0.862	$225.0x10^6$	$5.82x10^{-9}$	0.762
F-65	$7.08x10^3$	$2.10x10^6$	$8.30x10^{-10}$	0.829	$422.0x10^6$	3.72x10-^{9}	0.779

Table 4. Values of σ for films loaded with AgNPs calculated from EIS data.

SAMPLE	$\lambda_{max,1}$ (nm)	R_S (Ω mm^{-2})	d (mm)	σ (S cm^{-1})
PVA	---	65.6	0.0117	$1.71x10^{-9}$
F-00	416	18.1	0.0708	$3.76x10^{-8}$
F-40	515	53.6	0.079	$1.42x10^{-8}$
F-65	632	70.8	0.062	$8.42x10^{-9}$

4. Conclusions

The morphology of AgNPs is strongly influenced by the composition of the medium of synthesis, and the difference of their features can be evidenced by their optical properties. Nanostructures dispersions with a maximum in its plasmon absorption band at wavelength < 490 nm exhibited a yellow-red color, those with $\lambda_{max,1}$ between 482 - 515 nm exhibited a purple-blue color, while those with $\lambda_{max,1}$ between 533 - 632 nm exhibited a turquoise - green color. The shape of AgNPs undergoes a transition from spherical particles which were truncated, or faceted, as the amount of the precursor silver salt increased, increasing the size of the particles, until it reached polyhedral and even prism-like structures.

PVA films loaded with silver nanostructures with the different shapes described above were prepared and their electrical properties were studied. EIS measurements demonstrated that those systems' impedances could be accurately described by either a simple Randles circuit in the case of un-loaded PVA or by a modified Randles-type circuit which is complemented by grain-boundary effects. Nyquist plots of these systems demonstrate, together with the impedance plots, a clear dependence on the size and shape of the loading nanostructures. These differences demonstrated by the values of R_s account for the presence of an ionic dissociation system that affects the conductivity of the prepared samples. The importance of this dependence of the conductive properties of the polymer with the size and shape of the nanostructure will allow, in the near future, the development of polar ion-conducting polymers with custom conductivities. Furthermore, polymeric electrolytes loaded with metallic nanostructures are considered good candidates for the development of new photodynamic therapeutic treatments.

5. Acknowledgment

The authors would like to thank the internal projects (grants) CHEM19-10 and CHEM19-14 of Yachay Tech University for supporting this work and provide facilities required to carry out this work.

6. References

1. Hornyak GL, Tibbals HF, Dutta J, Moore JJ. Introduction to nanoscience and nanotechnology. 1st ed. Boca Raton: CRC Press Taylor; 2009. p. 4-52.
2. Talebian S, Wallace GG, Schroeder A, Stellacci F, Conde J. Nanotechnology-based disinfectants and sensors for SARS-CoV-2. Nat Nanotechnol. 2020;15(8):618-21.
3. Thiruvengadam M, Rajakumar G, Chung IM. Nanotechnology: current uses and future applications in the food industry. 3 Biotech. 2018;8(1):74.
4. Khatoon N, Mazumder JA, Sardar M. Current biotechnological applications of green synthesized silver nanoparticles. J. Nanosciences. 2017;2(1):1-8.
5. Beyene HD, Werkneh AA, Bezabh HK, Ambaye TG. Synthesis paradigm and applications of silver nanoparticles (AgNPs), a review. Sustainable Mater Technol. 2017;13:18-23.
6. Dobrucka R. Selected applications of metal nanoparticles in medicine and pharmacology. LogForum. 2019;15(4):449-57.
7. Wang C, Liu B, Dou X. Silver nanotriangles-loaded filter paper for ultrasensitive SERS detection application benefited by interspacing of sharp edges. Sens Actuators B Chem. 2016;231:357-64.
8. Schadler LS. Polymer-based and polymer-filled nanocomposites. In: Ajayan PM, Schadler LS, Braun PV, editors. Nanocomposite science and technology. Weinheim: Wiley-VCH; 2013. p. 119-27.
9. Shieh J-Y, Wu C-H, Tsai S-Y, Yu HH. Fabrication and characterization of a sandpaper-based flexible energy storage. Appl Surf Sci. 2016;364:21-8.
10. Kuznetsov IE, Akkuratov AV, Troshin PA. Polymer nanocomposites for solar cells: research trends and perspectives. In: Thomas S, Kalarikkal, N, Wu J, Mamour EH, Oluwatobi S, editors. Nanomaterials for solar cell applications. Amsterdam: Elsevier; 2019. p 557-600.
11. Suppan G, Briones-Macías M, Pazmiño-Arias E, Zamora-Ledezma C. Fabrication and characterization of metal-free composite electrodes based on few-layer-graphene nanoplatelets for oxygen reduction reaction applications. Phys Status Solidi, B Basic Res. 2021;258(5):2000515.
12. Goodship V, Cherrington R, Liang J. Materials and deposition processes for multifunctionality. In: Sina E, editor. Design and manufacture of plastic components for multifunctionality: structural composites, injection molding, and 3D printing. Amsterdam: Elsevier; 2016. p. 19-46. (PDL Handbook Series).
13. Alakanandana A, Subrahmanyam AR, Siva J. Structural and electrical conductivity studies of pure PVA and PVA doped with Succinic acid polymer electrolyte system. Mater Today Proc. 2016;3:3680-8.
14. Halima NB. Poly(vinyl alcohol): review of its promising applications and insights into biodegradation. RSC Advances. 2016;6(46):39823-32.
15. Hanemann T, Szabó DV. Polymer-nanoparticle composites: from synthesis to modern applications. Materials. 2010;3(6):3468-517.
16. Uddin MJ, Alaboina PK, Zhang L, Cho SJ. A low-cost, environment-friendly lignin-polyvinyl alcohol nanofiber separator using a water-based method for safer and faster lithium-ion batteries. Mater Sci Eng B. 2017;223:84-90.
17. Power A, Betts A, Cassidy J. Silver nanoparticle polymer composite based humidity sensor. Analyst. 2010;135(7):645-652.
18. Liang K-L, Wang Y-C, Lin W-L, Lin J-J. Polymer-assisted self-assembly of silver nanoparticles into interconnected morphology and enhanced surface electric conductivity. RSC Advances. 2014;4(29):15098.
19. Karthik S, Suresh J, Saravanan P, Arun A. Highly conducting solid electrolyte films based on PVA and iron alum: Synthesis, characterization and electrical properties. J Sci Adv Mater Devices. 2020;5(3):400-408.
20. Hemalatha KS, Sriprakash G, Ambika Prasad MVN, Damle R, Rukmani K. Temperature dependent dielectric and conductivity studies of polyvinyl alcohol-ZnO nanocomposite films by impedance spectroscopy. J Appl Phys. 2015;118(15):154103.
21. Nasar G, Azhar Khan M, Nadeem Q, Amin H, Ahmad N, ur Rehman J, et al. Silver-polymer nanocomposites: structural, thermal and electromechanical elucidation for charge storage applications. Measurement. 2020;156:107615.
22. Power A, Betts T, Cassidy H. The bench synthesis of silver nanostructures of variable size and an introductory analysis of their optical properties. Aust J Educ Chem. 2013;73.
23. Ramírez N, Regueiro A, Arias O, Contreras R. Espectroscopía de Impedancia Electroquímica: herramienta eficaz para el diagnóstico rápido microbiológico. Biotecnol Apl. 2009;26(1):65-71.
24. Anker JN, Hall WP, Lyandres O, Shah NC, Zhao J, van Duyne RP. Biosensing with plasmonic nanosensors. Nat Mater. 2008;7(6):442-453.

25. González A, Noguez C. Influence of morphology on the optical properties of metal nanoparticles. J Comput Theor Nanosci. 2007;4(2):231-8.
26. Jensen TR, Malinsky MD, Haynes CL, van Duyne RP. Nanosphere lithography: tunable localized surface plasmon resonance spectra of silver nanoparticles. J Phys Chem B. 2000;104(45):10549-56.
27. Huang ST, Xu XN. Synthesis and characterization of tunable rainbow colored colloidal silver nanoparticles using single-nanoparticle plasmonic microscopy and spectroscopy. J Mater Chem. 2010;20(44):9867-76.
28. Rivero PJ, Goicoechea J, Urrutia A, Arregui FJ. Effect of both protective and reducing agents in the synthesis of multicolor silver nanoparticles. Nanoscale Res Lett. 2013;8(1):101.
29. Aslan K, Lakowicz JR, Szmacinski H, Geddes CD. Enhanced ratiometric pH sensing using SNAFL-2 on silver island films: metal-enhanced fluorescence sensing. J Fluoresc. 2005;15(1):37-40.
30. Chen Y, Munechika K, Ginger DS. Dependence of fluorescence intensity on the spectral overlap between fluorophores and plasmon resonant single silver nanoparticles. Nano Lett. 2007;7(3):690-6.
31. Saade J, de Araújo CB. Synthesis of silver nanoprisms: a photochemical approach using light emission diodes. Mater Chem Phys. 2014;148(3):1184-93.
32. Nie S, Emory SR. Probing single molecules and single nanoparticles by surface-enhanced raman scattering. Science. 1997;275(5303):1102-6.
33. Emory SR, Nie S. Near-Field Surface-Enhanced Raman Spectroscopy on Single Silver Nanoparticles, S. Anal Chem. 1997;69(14):2631-5.
34. Xue B, Wang D, Zuo J, Kong X, Zhang Y, Liu X, et al. Towards high quality triangular silver nanoprisms: improved synthesis, six-tip based hot spots and ultra-high local surface plasmon resonance sensitivity. Nanoscale. 2015;7(17):8048-57.
35. Meulendijks N, Van Ee R, Stevens R, Mourad M, Verheijen M, Kambly N, et al. Flow cell coupled dynamic light scattering for real-time monitoring of nanoparticle size during liquid phase bottom-up synthesis. Appl Sci. 2018;8(1):108.
36. Mukherji S, Bharti S, Shukla G, Mukherji S. Synthesis and characterization of size- and shape-controlled silver nanoparticles. Physical Sciences Reviews. 2019;4(1):20170082.
37. Israelachvili JN. Intermolecular and surface forces. London: Academic Press; 2011. p. 326-34.
38. Frank AJ, Cathcart N, Maly KE, Kitaev V. Synthesis of silver nanoprisms with variable size and investigation of their optical properties: a first-year undergraduate experiment exploring plasmonic nanoparticles. J Chem Educ. 2010;87(10):1098-101.
39. Haes AJ, Haynes CL, van Duyne RP. Nanosphere lithography: self-assembled photonic and magnetic materials. Mat Res Soc Symp. 2001;636:481-6.
40. Paramelle D, Sadovoy A, Gorelik S, Free P, Hobley J, Fernig DG. A rapid method to estimate the concentration of citrate capped silver nanoparticles from UV-visible light spectra. Analyst. 2014;139(19):4855-61.
41. Sosa I, Noguez C, Barrera RG. Optical properties of nanoparticles and nanocomposites with arbitrary shapes. J Phys Chem B. 2003;107(26):6269-75.
42. Stetefeld J, McKenna SA, Patel TR. Dynamic light scattering: a practical guide and applications in biomedical sciences. Biophys Rev. 2016;8(4):409-27.
43. Liu H, Pierre-Pierre N, Huo Q. Dynamic light scattering for gold nanorod size characterization and study of nanorod–protein interactions. Gold Bull. 2012;45(4):187-95.
44. Hanemann T, Szabó DV. Polymer-nanoparticle composites: from synthesis to modern applications. Materials. 2010;3(6):3468-517.
45. Devikala S. Electrochemical performance of PVA/Al2O3 composite in 3.5% NaCl. Materials Today Proc. 2021;34(2):479-81.
46. Aziz SB, Mamand SM, Saed SR, Abdullah RM, Hussein SA. New method for the development of plasmonic metal-semiconductor interface layer: polymer composites with reduced energy band gap. J Nanomater. 2017;2017:8140693.
47. Aziz SB, Brza MA, Mohamed PA, Kadir MFZ, Hamsan MH, Abdulwahid RT, et al. Increase of metallic silver nanoparticles in Chitosan:AgNt based polymer electrolytes incorporated with alumina filler. Res Phys. 2019;13:102326.
48. Orazem M, Tribollet B. Electrochemical impedance spectroscopy. 2nd ed. Hoboken: John Wiley & Sons; 2008. p. 328-351.
49. Molleman B, Hiemstra T. Surface structure of silver nanoparticles as a model for understanding the oxidative dissolution of silver ions. Langmuir. 2015;31(49):13361-72.
50. Hdidar M, Chouikhi S, Fattoum A, Arous M. Effect of hydrolysis degree and mass molecular weight on the structure and properties of PVA films. Ionics. 2017;23(11):3125-35.
51. Rithin NB, Crasta V, Praveen BM. Dielectric and electric conductivity studies of PVA (Mowiol 10-98) doped with MWCNTs and WO3nanocomposites films. Mater Res Express. 2016;3(5):055012.
52. Mahendia S, Tomar AK, Kumar S. Electrical conductivity and dielectric spectroscopic studies of PVA-Ag nanocomposite films. J Alloys Compd. 2010;508(2):406-11.
53. Salman SA, Zainab AA, Zainab FN. Electrical properties of polyvinyl alcohol (PVA) films doped with $CoCl_2$ salt. Int J Curr Res. 2014;6(4):6225-7.